Multimodal Far-Field Acoustic Radiation Pattern Using Mode Cutoff Ratio

Edward J. Rice*
NASA Lewis Research Center, Cleveland, Ohio

The far-field sound radiation theory for a circular duct was studied for both single-mode and multimodal inputs. The investigation was intended to develop a method to determine the acoustic power produced by turbofans as a function of mode cutoff ratio. This information is essential for the design of acoustic suppressors in engine ducts. With reasonable simplifying assumptions, the single-mode radiation pattern was shown to be reducible to a function of mode cutoff ratio only (modal indices removed). With modal cutoff ratio as the dominant variable, multimodal radiation patterns can be reduced to a simple explicit expression. This approximate expression provides excellent agreement with an exact calculation of the sound radiation pattern using equal acoustic power per mode. Radiation patterns for cases other than equal modal power are presented using the approximate radiation equation. An approximate expression for the duct termination losses as a function of cutoff ratio also is included.

Nomenclature

c = speed of sound, m/s
D = duct diameter, m
$\mathfrak{D}$ = modal density function [see Eq. (15)]
f = frequency, Hz
I_T = acoustic intensity transmitted out from termination, N/ms
I_{inc} = acoustic intensity incident upon duct termination, N/ms
J'_m = derivative of the Bessel function of the first kind of order m with respect to its argument
k = side-lobe index [see Eq. (24)]
m = spinning mode lobe number (also order of Bessel function)
N = fraction of the total number of modes whose principal lobes contribute at any far-field position [see Eq. (16)]
n = exponent on cutoff ratio biasing function [see Eq. (18)]
P = far-field acoustic pressure amplitude [see Eq. (1)], N/m^2
P_D = acoustic pressure in the duct, N/m^2
P_m = P due to multimodal summation of principal lobes, N/m^2
P_p = P at the peak of the principal lobe, N/m^2
P_s = P due to side lobes, N/m^2
$\mathfrak{R}$ = reflection coefficient at duct termination
r = radial coordinate in cylindrical system, m
r_0 = radius of cylindrical duct, m
t = time, s
α = hard-wall duct mode eigenvalue [see Eq. (3)]
β = cutoff ratio biasing function [see Eq. (18)]
η = frequency parameter fD/c
θ_R = duct termination dimensionless acoustic radiation resistance
μ = radial mode number
ξ = mode cutoff ratio [see Eq. (4)]
ξ_{mic} = cutoff ratio for mode whose principal lobe peaks at a given far-field microphone position
ξ_{ps} = cutoff ratio for a particular side-lobe peaking at a given angle [see Eqs. (26) and (27)]
τ = propagation coefficient [see Eq. (21)]
ϕ = angular coordinate, rad
χ_R = duct termination dimensionless acoustic radiation reactance
ψ = far-field angle measured from inlet duct centerline, deg
ψ_p = ψ for the peak of the principal lobe [see Eq. (9)]
ψ_{ps} = ψ for the peak of the side lobes [see Eq. (24)]
ω = circular frequency, rad/s

Presented as Paper 77-1281 at the AIAA 4th Aeroacoustics Conference, Atlanta, Ga., Oct. 3-5, 1977; submitted Dec. 1, 1977; revision received April 17, 1978. Copyright © American Institute of Aeronautics and Astronautics, Inc., 1977. All rights reserved.

Index categories: Noise; Aeroacoustics.

*Head, Acoustics Section. Member AIAA.

Introduction

THE far-field acoustic radiation pattern produced by a single mode in a circular duct has been presented for flanged ducts[1-3] as well as for unflanged ducts.[3,4] Multimodal radiation patterns representing the summation of the contributions of the many modes have been studied.[5] Besides being very time consuming, it was not obvious how cases other than equal acoustic power or amplitude per mode could be handled using exact calculations for the multimodal case. A method is presented here which makes this calculation possible by using a cutoff ratio biasing function.

This paper presents an analysis in which the single-mode radiation equations can be summed analytically into a multimodal radiation pattern. The single-mode theory is first simplified into a function only of mode cutoff ratio, which means that the actual modal identification is suppressed, and all modes with approximately the same cutoff ratio will have approximately the same radiation pattern. A modal density function, which is also a function only of mode cutoff ratio, is used to estimate the number of modes significantly contributing to the pressure at a far-field observation point. The single-mode pressure amplitude and number of modes contributing are then combined to give a resultant mean-square pressure at the far-field observation point. This procedure yields a simple explicit expression, which is then compared to exact calculations using equal power per mode. The extension to the more general case of unequal power per mode is also presented. An approximate expression for the duct termination loss as a function of cutoff ratio is developed. Calculations using the multimodal far-field radiation expressions are compared with experimental data.

The concept that the far-field radiation pattern is a function of acoustic power vs mode cutoff ratio is useful for acoustic linear design purposes. The propagation of sound through lined ducts has previously been shown to be a function of cutoff ratio.[6,7] The work presented here represents a part of a simplified acoustic linear design program under development.

The noise source information needed for the linear design can be obtained directly from the far-field radiation pattern.

Analysis Technique and Results

The single-mode far-field acoustic radiation expression will first be developed as a function of cutoff ratio. The summation required for the multimode case will then be derived. The equations without steady flow will be used here as an illustration.

A far-field mean-squared pressure radiation expression for a flanged circular duct for equal acoustic power per mode[5] can be expressed as

$$P^2 = \frac{(\pi\eta)^3\sqrt{(\pi\eta)^2-\alpha^2}\sin^2\psi[J'_m(\pi\eta\sin\psi)]^2}{[1-(m/\alpha)^2][\alpha^2-(\pi\eta\sin\psi)^2]^2} \tag{1}$$

where the frequency parameter η is

$$\eta = fD/c \tag{2}$$

and the mode eigenvalue α is determined from

$$J'_m(\alpha) = 0 \tag{3}$$

Equation (1) was derived for zero Mach number and negligible end reflections, and a constant has been omitted. Note that subscripts m, μ should occur on P^2 and α to denote the lobe number m and the radial mode index μ, but they are omitted here for brevity.

Let the mode cutoff ratio be defined as

$$\xi = \pi\eta/\alpha \tag{4}$$

which is consistent with previous results.[2,8] Using Eq. (4) in Eq. (1) yields

$$P^2 = \frac{\sin^2\psi\sqrt{1-1/\xi^2}[J'_m(\pi\eta\sin\psi)]^2}{[1-(m/\alpha)^2][1/\xi^2-\sin^2\psi]^2} \tag{5}$$

Note that in Eq. (5) the modal identity remains in the m/α term and in the Bessel function order m. Two assumptions are made. First,

$$(m/\alpha)^2 \ll 1 \tag{6}$$

and second,

$$J'_m(\pi\eta\sin\psi) \approx -\sqrt{2/\pi^2\eta\sin\psi}\sin(\pi\eta\sin\psi-\alpha) \tag{7}$$

which can be obtained from published expressions.[9]

Equations (6) and (7) are valid except for the first few radial orders of the higher lobe number modes. Using Eqs. (4, 6, and 7) in Eq. (5) yields

$$P^2 \approx \frac{2\sin\psi\sqrt{1-1/\xi^2}\{\sin[\pi\eta(\sin\psi-1/\xi)]\}^2}{\pi^2\eta[1/\xi^2-\sin^2\psi]^2} \tag{8}$$

Equation (8) shows that the radiation pattern is a fucntion of cutoff ratio (ξ) only and that modal identity has been suppressed, being now implicitly involved in ξ. The frequency parameter η of course remains, but this involves only the usual inputs of frequency and duct diameter D. Provided that conditions given by Eqs. (6) and (7) are not violated radically, all modes with the same cutoff ratio have identical radiation patterns. One difference between the approximate Eq. (8) and the more exact Eq. (1) occurs in the number of side lobes occurring forward ($\psi < \psi_p$) of the principal lobe. Equation (8) shows that, for a given cutoff ratio ξ and frequency parameter η, there are a constant number of these side lobes. However, for Eq. (1) the number of these side lobes is dependent upon the radial mode number μ. This error occurs due to the difference between the small argument behavior of the sine function and the Bessel function. Since the side lobes are generally 10 to 15 dB below the principal lobe, this error in the forward side lobes is of little consequence in a multimodal radiation pattern.

From Eq. (8), it can be seen that both the numerator and the denominator go to zero when

$$\sin\psi_p = 1/\xi \tag{9}$$

which approximately defines the location of the principal lobe peak pressure. The subscript p has been added to ψ to signify the angle for the peak pressure. A limiting procedure on Eq. (8) yields for the magnitude of the principle lobe:

$$P_p^2 \approx \frac{\eta\xi\sqrt{1-1/\xi^2}}{2} = \frac{\eta\cos\psi_p}{2\sin\psi_p} \tag{10}$$

where Eq. (9) was also used. The same result occurs using the exact Eq. (1) if the approximation of Eq. (6) is used.

Equation (8) also shows that the principal lobe extends between angles

$$\sin\psi \approx (1/\xi) - (1/\eta) \tag{11}$$

and

$$\sin\psi \approx (1/\xi) + (1/\eta) \tag{12}$$

which represent the first zeros of $\sin[\pi\eta(\sin\psi - 1/\xi)]$ about the peak.

Multimodal Radiation Pattern

Equal Acoustic Power per Mode

Consider a far-field location, say a microphone location, described by the angle ψ. With a multitude of modes present, there is some mode with a cutoff ratio ξ whose principal lobe peaks at this location. The principal lobe of this mode is shown as the solid line, with cutoff ratio shown as ξ_{mic} in Fig. 1. Also there are many other modes whose peaks are not at ψ but whose principal lobe still contributes to the pressure at ψ. Samples of such modes are shown as the dashed lines in Fig. 1. The dash-dot curves show the extreme values of cutoff ratio beyond which no contribution to the microphone pressure is made by the principal lobes. The range of cuttoff ratios that have some principal lobe contribution at ψ can be found from Eqs. (11) and (12) to be

$$1/\xi_1 \approx \sin\psi - (1/\eta) \tag{13}$$

to

$$1/\xi_2 \approx \sin\psi + (1/\eta) \tag{14}$$

The number of modes in this cutoff range can be estimated using the modal density function[10]:

$$\mathfrak{D} \approx 2/\xi^3 \tag{15}$$

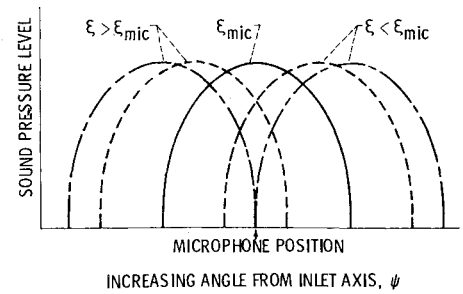

Fig. 1 Schematic of modal principle lobes of radiation contributing to a far-field microphone signal.

This is a density function in the usual sense in that an integration must be performed to obtain the number of modes. The most desirable way of obtaining the microphone pressure signal is to multiply Eq. (8) by the modal density function and integrate over cutoff ratio between zero and infinity. Since this cannot be done in closed form, a simpler procedure will be used. Integration of Eq. (15) between the limits given by Eqs. (13) and (14) yields

$$N=\int_{\xi_2}^{\xi_1}\mathfrak{D}d\xi=\frac{4}{\eta\xi}=\frac{4\sin\psi}{\eta} \tag{16}$$

which represents the fraction of the total number of modes whose principal lobes contribute to the pressure at angle ψ. The simplest possible way of integrating the amplitude and mode number effects is to multiply Eq. (10) by Eq. (16) to yield

$$P_m^2\approx 2\cos\psi \tag{17}$$

Equation (17) is seen to be a simple expression for the far-field pressure at any angle ψ due to many modes with equal acoustic power per mode. In Fig. 2, Eq. (17) is compared to an exact calculation using an exact summation of Eq. (1) for over 1000 modes.[11] The agreement between the exact and approximate calculations is seen to be excellent. This justifies the approximations made earlier.

Unequal Acoustic Power per Mode

It is desirable to have a simple expression comparable to Eq. (17) for other than equal acoustic power per mode. It also is of interest to alter the expression so as to keep it a function of cutoff ratio, since propagation in acoustic liners has been correlated with cutoff ratio.[6,7] A cutoff ratio biasing function can be defined as

$$\beta=1/\xi^n \tag{18}$$

where the exponent n serves to alter the acoustic power distribution as a function of cutoff ratio which represents a modal power shift. Equation (1) can be multiplied by the cutoff ratio biasing function $1/\xi^n$ to produce a shift in acoustic power away from equal power per mode ($n=0$). This is not the only biasing function that could be used, but it is both simple and convenient in form and will be used in this initial effort. Exact calculations of the sum of the mean-square pressure at any microphone position (fixed ψ) could be made by summing over all of the propagating modes (varying eigenvalue α) with the cutoff ratio used for each mode to calculate the power biasing function.

As in the case of equal acoustic power per mode, instead of performing the exact calculation just outlined, a simpler procedure will be used to approximate the summation over modes or integration over cutoff ratio. First Eq. (10) for the principal mode peak value is multiplied by the cutoff ratio biasing function to yield

$$P_p^2\approx\frac{\eta\xi\sqrt{1-1/\xi^2}}{2\xi^n}=\frac{\eta\xi^{1-n}}{2}\sqrt{1-1/\xi^2} \tag{19}$$

Equation (19) then is multiplied by the number of modes [Eq. (16)] whose principal lobes can contribute to the mean-square pressure at the far-field angle ψ. This results in

$$P_m^2\approx 2\cos\psi\sin^n\psi \tag{20}$$

Figure 3 shows a plot of Eq. (20) for four values of the exponent n. As n is increased, the acoustic power distribution is shifted toward cutoff ($\xi=1$), and the radiation pattern peaks toward higher angles, with a noticeable reduction in the power near the inlet axis. The peak value of Eq. (20) is located at $\tan\psi=\sqrt{n}$.

The biasing function ($1/\xi^n$) used here is desirable for $n\geq 0$ but is not completely satisfactory for $n<0$. In the latter case, no absolute maximum occurs, and the mean-square pressure near the inlet axis continually increases as n is reduced (made larger negative). As mentioned previously, this first attempt at the biasing function was made for convenience, and further experimentation must be performed when making quantitative fits to real data. Qualitative fits to several sets of data will be shown after reflection from the duct termination effects and the contribution of side lobes have been included in the radiation pattern.

Modal Phasing Considerations

Note that in Eq. (1), the starting point for this analysis, only the pressure-squared term was considered. Also, in the development of Eqs. (17) and (20), the squared pressures from many modes were added together to obtain a resultant pressure-squared term. This squaring of the pressure eliminates possible pressure cancellations between the modes. The modes thus are assumed to be uncorrelated in phase, as might be expected with broadband noise or even for tones produced by random inflow directions.

For a tone that has only a few highly correlated duct modes associated with it, cancellations of pressure among the modes may be significant for the determination of the far-field pressure pattern. The far-field acoustic power flux could be represented by the square of the sum of the modal pressures, and this probably would not be equal to the sum of the

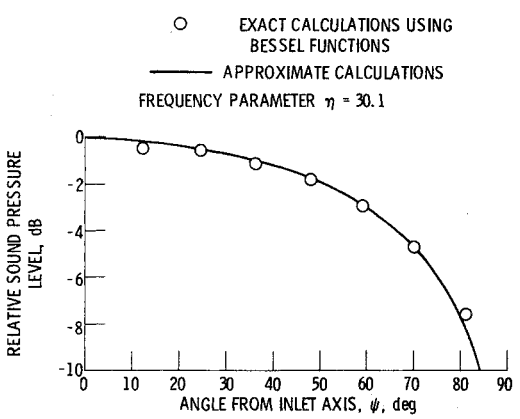

Fig. 2 Comparison of exact and approximate multimodal far-field directivity patterns for equal acoustic power per mode.

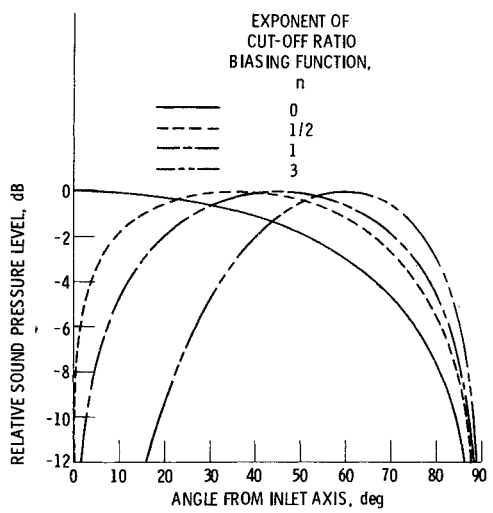

Fig. 3 Far-field multimodal directivity variation with cutoff ratio bias function exponent.

squares of the individual modal pressures. Thus, for this case of a few highly correlated modes, the method presented in this paper would not be valid. Fortunately, for this special case individual modal measurements in the duct may be possible.

Duct Termination Loss as a Function of Cutoff Ratio

The acoustic power loss (due to reflection) at the duct termination will be determined for each individual mode. Thus modal interactions as considered by Zorumski[12] will be neglected, and the results are only approximate. The power loss will be shown to be a function of cutoff ratio.

The pressure in the circular duct has the form

$$P_D = e^{i\omega t - in\phi}[e^{-i\omega\tau x/c} + \Re e^{+i\omega\tau x/c}]J_m(\alpha r/r_0) \tag{21}$$

where

$$\tau = \sqrt{1-(\alpha/\pi\eta)^2} = \sqrt{1-1/\xi^2} \tag{22}$$

given in terms of mode eigenvalue and cutoff ratio. Note that hard walls and zero axial Mach number are used here for simplicity. The reflection coefficient $\Re$ in Eq. (21) accounts for the reflection back from the duct termination which represents acoustic power lost to the farfield. The boundary condition at the duct end, in terms of radiation resistance θ_R and reactance χ_R, is used to evaluate $\Re$. The ratio of transmitted to incident acoustic power intensity can then be evaluated as

$$\frac{I_T}{I_{inc}} = \frac{4\tau\theta_R}{(1+\tau\theta_R)^2 + (\tau\chi_R)^2} \tag{23}$$

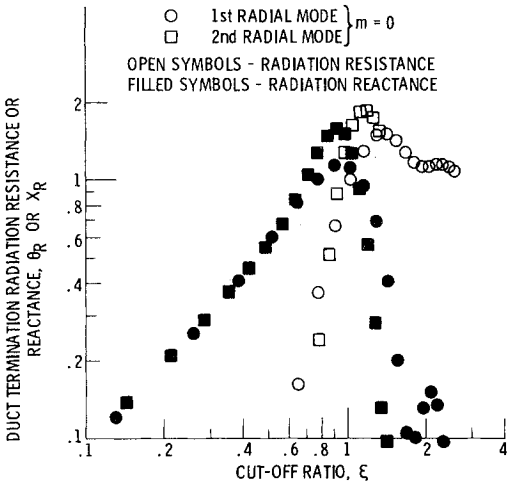

Fig. 4 Variation of duct termination radiation impedance components with cutoff ratio.

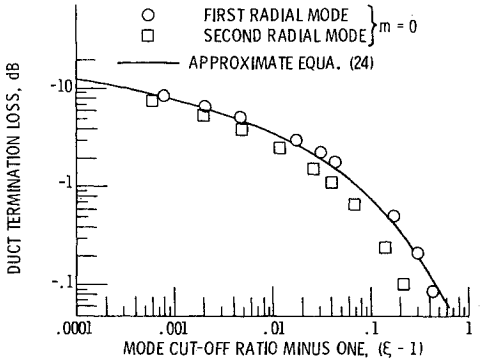

Fig. 5 Modal transmission loss at duct termination.

The radiation impedance components (θ_R and χ_R) for the first two axisymmetric ($m=0$) radial modes are plotted in Fig. 4. These calculations were made using the method of Ref. 12. Note that, when these calculated impedance components are plotted vs mode cutoff ratio, the results for the two modes are almost coincident. In addition, radiation impedance calculations for spinning modes were presented in Ref. 13 plotted as a function of nondimensional frequency minus cutoff frequency. These calculations showed the same trends as shown in Fig. 4. The impedance components rapidly increase through cutoff ($\xi=1$), with only minor variations among modes in the oscillatory parts of the curves beyond the cutoff point. This implies that the radiation impedance is approximately dependent only on cutoff ratio. Also note in Eq. (23) that the remaining term τ is a function only of cutoff ratio [see Eq. (22)]. Thus the duct termination loss is approximately only a function of cutoff ratio.

Calculations using Eq. (23) and the radiation impedance components of Fig. 4 are shown in Fig. 5. The slight difference in radiation impedance components causes a small difference in termination loss. A further approximation will be made, completely ignoring the small differences in radiation impedance among modes (when considered as a function of cutoff ratio). For relatively large cutoff ratios, $\theta_R \to 1$ and $\chi_R \to 0$. Using these values in Eq. (23) yields

$$I_T/I_{inc} \approx 4\tau/(1+\tau)^2 \tag{24}$$

Equation (24) is purely a function of cutoff ratio and is plotted vs $(\xi-1)$ as the solid line in Fig. 5. This approximate relationship is seen to describe adequately the termination loss calculations shown in Fig. 5 and, due to the previously described results of Ref. 13, is expected to provide an adequate result for all of the modes. It can be seen in Fig. 5 that the duct termination loss is large only near mode cutoff. For cutoff ratios greater than 1.1, the loss is less than 1 dB. Equation (24) has been used for the termination loss for the results that are presented in later figures.

The termination loss thus joins the list of duct lining phenomena that appear to be approximately related only to mode cutoff ratio. These include acoustic linear modal optimum impedance and maximum possible attenuation[6,7] and modal far-field radiation pattern [Eq. (8)].

Effect of Side Lobes on Multimodal Radiation Pattern

As previously discussed, the side lobes in the radiation pattern have considerably lower amplitude than the principal lobe and were ignored in the approximate calculations presented in Figs. 1 and 2. They were, of course, automatically contained in the exact calculations of Fig. 1 and are seen to have very little effect. However, when the termination loss is included which mainly reduces the principal lobes at higher angles (near cutoff), the radiation pattern is dominated by the side lobes from modes whose principal lobes fall nearer to the inlet axis (well-propagating modes with larger cutoff ratios). Also, when duct liners are included, the principal lobes may be reduced drastically over a far-field angle range, and a noise floor results from the side lobes of the less attenuated modes. The side lobes are thus included in the results shown later in this paper.

Equation (8) shows that the kth side lobe (counting from the principal lobe) peaks at the angle ψ_{ps}, given by

$$\sin\psi_{ps} = \frac{1}{\xi} \pm \frac{(2k+1)}{2\eta}, \quad k=1,2,3... \tag{25}$$

where the plus and minus signs take care of side lobes at angles greater than and less than that of the principal lobe. Equation (25) is the parallel of Eq. (9) for the principal lobe. Using Eq. (25) and using a procedure similar to that used for the principal lobe, the number of modes whose kth side lobe

contributes to the mean-square pressure at the far-field angle ψ is determined as

$$N_S = 2/\eta\xi_{ps} \tag{26}$$

where ξ_{ps} is the cutoff ratio of the mode whose kth side lobe peaks at the angle ψ and is given by

$$\frac{1}{\xi_{ps}} = \sin\psi - \frac{(2k+1)}{2\eta}, \quad k \le \eta\sin\psi - \tfrac{1}{2} \tag{27}$$

for side lobes above the principal lobe, and

$$\frac{1}{\xi_{ps}} = \sin\psi + \frac{(2k+1)}{2\eta}, \quad k \le \eta(1-\sin\psi) - \tfrac{1}{2} \tag{28}$$

for side lobes below the principal lobe. Finally, the multimodal contribution of the kth side lobe is

$$P_s^2 = \frac{4\sin\psi\sqrt{1-1/\xi_{ps}^2}}{\pi^2\eta^2\xi_{ps}^{n+1}[1/\xi_{ps}^2 - \sin^2\psi]^2} \tag{29}$$

A summation over the side lobes is required using Eqs. (27) and (28).

Comparison of Calculated Radiation Patterns with Experimental Data

Several sets of experimental radiation directivity patterns will be compared to the calculated patterns derived in the previous sections. Although the ultimate intent of this work is to infer the acoustic power distribution as a function of cutoff ratio, this has not been done rigorously here. The cutoff ratio biasing function is considered preliminary and for illustrative purposes only at this time. Several interesting qualitative features of the data-theory comparisons, however, will be pointed out.

In Fig. 6, four sets of data considered to be broadband noise[14] are plotted. Only inlet noise is present, since aft noise is ducted away. The solid curve represents the multimodal equal power per mode theory, with the biasing exponent equal to zero ($n=0$). The comparison of the data with the theory shows this broadband noise to be very close to equal acoustic power per mode. The data are seen to be almost unchanged when the tunnel flow is added. Equal power per mode is a very appealing result for broadband noise, since this usually is associated with random processes.

Figure 7 shows some broadband data[15] for the NASA fan B on a static outdoor test stand. These data have been analyzed carefully to remove the multiple pure tones from the broadband contribution.[15] Also, an attempt has been made to remove the radiated noise contributed from the fan aft duct or jet. A comparison of the data with the equal acoustic power per mode calculation shows the data to agree very well with this curve. Thus, for the two different fans tested in two different facilities, as represented by Figs. 6 and 7, the broadband noise radiation patterns appear to be very close to that expected for equal acoustic power per mode.

Blade passage frequency data from two fans statically tested at two speeds are shown in Fig. 8. Although there is some scatter in the data, the trends fit relatively well with the theoretical curves shown with $n=\frac{1}{2}$ or 1. These data are shifted away from equal power ($n=0$) toward cutoff. This is evident from the higher radiation at larger angles and the reduced radiation toward the inlet axis.

A sample of the blade passage frequency directivity data for the Lycoming YF-102 engine tested at NASA Lewis is shown in Fig. 9. The solid curve is the multimodal theory for equal

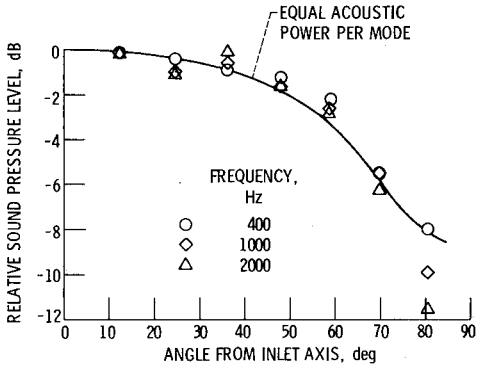

Fig. 7 Comparison of equal power per mode multimodal directivity to experimental data from NASA fan B.[15]

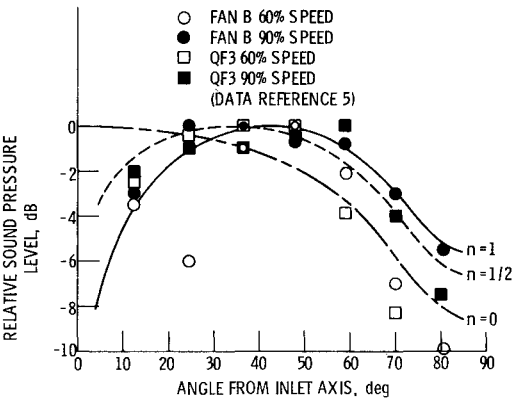

Fig. 8 Comparison of fan blade passage frequency data with calculated far-field multimodal directivity patterns.

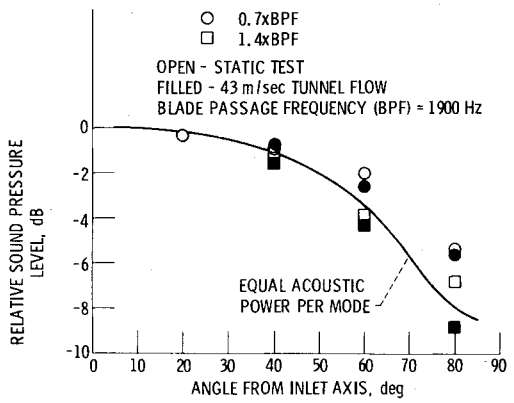

Fig. 6 Comparison of multimodal equal power per mode directivity to experimental data obtained in a wind tunnel.[14]

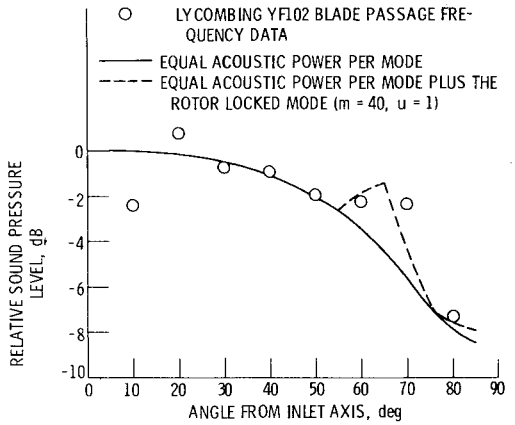

Fig. 9 Comparison of experimental data with calculated multimodal directivity pattern.

acoustic power per mode. Except for small aberrations near the axis and centered at 65 deg, the curve fits the data very well. The deviation at 65 deg may represent the contribution of an additional single mode, the rotor-locked mode with 40 lobes ($m=40$). Only the first radial order of this mode can propagate. The dashed line represents the adding of this mode to the theoretical curve. This helps to explain the deviation at the higher angles. This illustrates a reasonable procedure that probably can be used in future data analysis. After deviations in the radiation pattern have been determined to be truly valid, a limited number of physically sensible modes may be added to the underlying smooth multimodal radiation pattern. No attempt has been made to explain the deviations of the data near the axis.

This very limited comparison of data with theory has pointed out that a variety of acoustic power vs cutoff ratio (or modal) distributions are to be expected from experimental data. Some of the differences might be due to different fan designs or to different experimental test installations.

Concluding Remarks

A simple explicit equation has been derived for multimodal far-field acoustic radiation from a flanged circular duct for arbitrary acoustic power/cutoff ratio distribution. The approximate expression agrees very well with exact calculations when equal acoustic power per mode is specified. The approximate expression was based upon only the principal lobes of the modal radiation pattern, but additional expressions are provided to account for the side lobes in cases where they must be included. The derivation used an approximate integration of a continuously distributed modal distribution which certainly will be of questionable validity if only a few modes are propagating.

Approximate expressions for the single-mode far-field radiation pattern and duct termination loss were presented. Exact modal identification has been suppressed in these two expressions, and they have been shown to be functions only of the modal cutoff ratio. This is convenient, since previously it has been shown that the sound propagation in the noise suppressor itself is predominantly a function only of cutoff ratio.

Several sets of experimental data for inlet radiated noise were compared to theoretical curves. This comparison, although qualitative at this time, has shown that a variety of acoustic power/cutoff ratio distributions might be expected. These may depend upon the spectral nature (tone or broadband) of the noise, the fan characteristics, or the test installation. Some distributions are fairly smooth vs angle, while some may require the addition of some physically sensible modes.

References

[1] Morse, P. M., *Vibration and Sound*, McGraw-Hill, New York, 1948.

[2] Tyler, J. M. and Sofrin, T. G., "Axial Flow Compressor Noise Studies," *SAE Transactions*, Vol. 70, 1962, pp. 309-332.

[3] Lansing, D. L., Drischler, J. A., and Pusey, C. G., "Radiation of Sound from an Unflanged Circular Duct with Flow," *79th Meeting of the Acoustical Society of America*, Atlantic City, N.J., April 21-24, 1970.

[4] Homicz, G. F. and Lordi, J. A., "A Note on the Radiative Directivity Patterns of Duct Acoustic Modes," *Journal of Sound and Vibration*, Vol. 41, Aug. 1975, pp. 283-290.

[5] Saule, A. V., "Modal Structure Inferred from Static Far-Field Noise Directivity," AIAA Paper 76-574, Palo Alto, Calif., 1976.

[6] Rice, E. J., "Acoustic Liner Optimum Impedance for Spinning Modes with Mode Cut-off Ratio as the Design Criterion," AIAA Paper 76-516, Palo Alto, Calif., 1976.

[7] Rice, E. J., "Inlet Noise Suppressor Design Method Based Upon the Distribution of Acoustic Power with Mode Cutoff Ratio," NASA CP-2001, Vol. 3, 1976, p. 883.

[8] Sofrin, T. G. and McCann, J. F., "Pratt and Whitney Experience in Compressor-Noise Reduction," Acoustical Society of America, Los Angeles, Calif., Preprint 2D2, 1966.

[9] Abramowitz, M. and Stegun, I. A., *Handbook of Mathematical Tables*, Dover, New York, 1965.

[10] Rice, E. J., "Modal Density Function and Number of Propagating Modes in Ducts," NASA TM X-73539, 1976.

[11] Saule, A. V. and Rice, E. J., "Far-Field Multimodal Acoustic Radiation Directivity," NASA TM-73839, Dec. 1977.

[12] Zorumski, W. E., "Generalized Radiation Impedances and Reflection Coefficients of Circular and Annular Ducts," *Journal of the Acoustical Society of America*, Vol. 54, Dec. 1973, pp. 1667-1673.

[13] Morfy, C. L., "A Note on the Radiation Efficiency of Acoustic Duct Modes," *Journal of Sound and Vibration*, Vol. 9, 1969, pp. 367-372.

[14] Dietrich, D. A., Heidmann, J. M., and Abbott, J. M., "Fan Acoustic Signatures of an Anechoic Wind Tunnel," *Journal of Aircraft*, Vol. 14, Nov. 1977, pp. 1109-1116; also AIAA Paper 77-59, Los Angeles, Calif., 1977.

[15] Saule, A. V., "Some Observations about the Components of Transonic Fan Noise from Narrow-Band Spectral Analysis," NASA TN D-7788, 1974.